Full-field response monitoring in structural systems driven by a set of identified equivalent forces

Lourens, E.; Fallais, D. J.M.

DOI
10.1016/j.ymssp.2018.05.014

Publication date
2019

Document Version
Accepted author manuscript

Published in
Mechanical Systems and Signal Processing

Citation (APA)
Lourens, E., & Fallais, D. J. M. (2019). Full-field response monitoring in structural systems driven by a set of identified equivalent forces. *Mechanical Systems and Signal Processing*, *114*, 106-119. https://doi.org/10.1016/j.ymssp.2018.05.014

Full-field response monitoring in structural systems driven by a set of identified equivalent forces

E. Lourens, D.J.M. Fallais

Faculty of Civil Engineering and GeoSciences, Delft University of Technology, Stevinweg 1, 2628 CN Delft, The Netherlands

Abstract

Kalman-type filters for coupled input-state estimation can be used to estimate the full-field dynamic response of structures from only a limited set of vibration measurements. The use of these coupled estimators allows for response prediction to be performed in the absence of any knowledge of both the dynamic evolution and spatial distribution of the excitation forces, where often a set of response-driving equivalent forces is identified from the measurements. In this contribution, a rigorous analysis of the concept of equivalent force based response monitoring is performed, with the aim to clearly establish its limitations and ranges of applicability. It is shown that, unlike commonly assumed, the success of this type of response monitoring cannot be related solely to whether the chosen set of equivalent forces satisfy the controllability requirements, but will depend on the bandwith of the excitation forces in combination with the extent/characteristics of the sensor network. Arguments are instantiated using simple numerical examples where a comparison is made between the theoretical assumptions used to derive the filters and the physical situation. Included in the analyses are situations where a) the applied and equivalent loads are concentrated and collocated, b) the applied and equivalent loads are concentrated and non-collocated, c) modal equivalent loads are used to represent concentrated non-moving forces, and d) modal equivalent loads are used to represent concentrated moving forces. Results are applicable to any Kalman-type coupled input-state estimator derived using the principles of minimum-variance unbiased estimation.

Keywords: response prediction, controllability, equivalent forces, Kalman filter, joint input-state estimation, structural health monitoring

E-mail address: e.lourens@tudelft.nl (E. Lourens).

1. Introduction

The problem of reconstructing the dynamic states of a system from sparse vibration measurements is considered, thereby contributing to ongoing research in the area of full-field response estimation on the basis of output-only data. The full-field response estimates are most commonly used for the purpose of monitoring fatigue damage accumulation in the entire body of large-scale structures [1, 2, 3], but can also be used to obtain valuable insights into complex interaction phenomena, e.g. ice-induced vibrations [4, 5], when monitored in conjunction with the applied forces.

In recent years, a large number of inverse methodologies for the extrapolation of locally measured structural response to unmeasured locations – through the estimation of full-field quantities – have been proposed. These methodologies can roughly be divided into two categories, namely those that assume that the numerical model used for the extrapolation is free from errors, and those that do account for modelling errors. Belonging to the former category are the modal expansion algorithms, where modal coordinates are identified through a pseudo-inversion of the mode shape matrix. These approaches work well for dynamic systems characterized by relatively low-order dynamic behavior, e.g. the supporting structures of offshore wind turbines [6, 7]. The second category consists of various Kalman-type filters, where modelling as well as measurement errors are included in the estimation as stochastic processes of which only the variances are known. Various state, coupled input-state, and coupled input-state-parameter estimation algorithms have been developed in this context, ranging from initial formulations for use with linear systems to alternative filters for dealing with reduced-order models, acceleration-only data and recently also nonlinear model descriptions. Limiting the discussion to linear systems, again two groups of filters can be distinguished: those that rely on some assumptions regarding the loading on the structure (e.g. white noise, or characterized by a certain known variance) [1, 8, 9], and those that are able to observe full-field structural response in the absence of any knowledge of the dynamic evolution of the applied loading [10, 11, 12].

In this contribution, we will focus on the second category presented above, namely the Kalman-type filters, and more specifically on cases in which also the spatial distribution of the loading is assumed unknown, and a set of response-driving equivalent forces is identified from the measurements. This is done when the locations of the main excitation sources are uncertain and/or time-varying, which is often the case for large-scale civil or offshore structures. Through a careful analysis of the assumptions forming the basis for the derivation of these algorithms and their possible violation in various real-life applications, the limitations of response estimation based on the concept of equivalent loading is exemplified. Up to now, the success of this type of equivalent force based response estimation has been related only to whether the chosen driving forces satisfy the controllability requirements [13]. It will be shown that controllability is an insufficient criterion for guaranteeing the accuracy of the response

estimates, and that results remain sensitive to a correct assumption on the force locations, unless the sensor network allows for the identification of a sufficiently large number of modal forces. Concepts are illustrated using simple numerical examples where a comparison is made between the true and assumed noise statistics and the response prediction accuracy for a number of distinct cases in which the locations of the forces are only known approximately, or not at all, in which case modal equivalent forces are assumed.

The paper is structured as follows: first the state-space notations which will be required for the definition of the necessary error statistics are presented in section 2, followed by a summary of the Kalman-type filters to which the results will apply and the assumptions forming the basis for their derivation in section 3. Section 4 presents the concept of equivalent force based response monitoring, and includes the development of new notation for quantifying discrepancies between the theoretical assumptions used to derive the filters and the true physical situation. The latter notations are then used in a set of numerical examples in section 5, on which basis conclusions are drawn for a selection of commonly encountered engineering problems in section 6.

2. Formulation of the state-space equations

The formulations presented in this section can be found in many references; we use the notation from [11], repeated here for convenience. The equations of motion for a linear system discretized in space are formulated as:

$$\mathbf{M}\ddot{\mathbf{u}}(t) + \mathbf{C}\dot{\mathbf{u}}(t) + \mathbf{K}\mathbf{u}(t) = \mathbf{f}(t) = \mathbf{S}_{\mathrm{p}}(t)\mathbf{p}(t) \tag{1}$$

where $\mathbf{u}(t) \in \mathbb{R}^{n_{\mathrm{DOF}}}$ is the vector of displacement, $\mathbf{M}$, $\mathbf{C}$ and $\mathbf{K} \in \mathbb{R}^{n_{\mathrm{DOF}} \times n_{\mathrm{DOF}}}$ denote the mass, damping and stiffness matrix, respectively, and $\mathbf{f}(t)$ is the excitation vector. The excitation is factorized into a force influence matrix $\mathbf{S}_{\mathrm{p}} \in \mathbb{R}^{n_{\mathrm{DOF}} \times n_{\mathrm{p}}}$, and the vector $\mathbf{p}(t) \in \mathbb{R}^{n_{\mathrm{p}}}$ representing the n_{p} force time histories. Each column of the matrix $\mathbf{S}_{\mathrm{p}}$ gives the spatial distribution of the load time history in the corresponding element of the vector $\mathbf{p}$. In the case of a point load, the column of $\mathbf{S}_{\mathrm{p}}$ has only a limited number of non-zero entries corresponding to the distribution of the load over the degrees of freedom of the FE mesh. In Eq. (1) $\mathbf{S}_{\mathrm{p}}$ is shown as being time dependent to allow also for the case of moving loads.

By introducing the state vector $\mathbf{x}(t) \in \mathbb{R}^{n_{\mathrm{s}}},\ n_{\mathrm{s}} = 2n_{\mathrm{DOF}}$:

$$\mathbf{x}(t) = \begin{pmatrix} \mathbf{u}(t) \\ \dot{\mathbf{u}}(t) \end{pmatrix}$$

the second-order equations of motion (1) can be written in first-order state space form:

$$\dot{\mathbf{x}}(t) = \mathbf{A}_{\mathrm{c}}\mathbf{x}(t) + \mathbf{B}_{\mathrm{c}}\mathbf{p}(t) \tag{2}$$

where the system matrices $\mathbf{A}_{\mathrm{c}} \in \mathbb{R}^{n_{\mathrm{s}} \times n_{\mathrm{s}}}$ and $\mathbf{B}_{\mathrm{c}} \in \mathbb{R}^{n_{\mathrm{s}} \times n_{\mathrm{p}}}$ are defined as:

$$\mathbf{A}_\mathrm{c} = \begin{bmatrix} \mathbf{0} & \mathbf{I} \\ -\mathbf{M}^{-1}\mathbf{K} & -\mathbf{M}^{-1}\mathbf{C} \end{bmatrix},\ \mathbf{B}_\mathrm{c} = \begin{bmatrix} \mathbf{0} \\ \mathbf{M}^{-1}\mathbf{S}_\mathrm{p} \end{bmatrix}$$

and the subscript 'c' denotes continuous time. The classical continuous-time state space description of the vibrating system is subsequently found by supplementing the state equation (2) with the so-called observation equation:

$$\mathbf{d}(t) = \mathbf{G}_\mathrm{c}\mathbf{x}(t) + \mathbf{J}_\mathrm{c}\mathbf{p}(t) \tag{3}$$

in which

$$\mathbf{G}_\mathrm{c} = \begin{bmatrix} \mathbf{S}_\mathrm{d} - \mathbf{S}_\mathrm{a}\mathbf{M}^{-1}\mathbf{K} & \mathbf{S}_\mathrm{v} - \mathbf{S}_\mathrm{a}\mathbf{M}^{-1}\mathbf{C} \end{bmatrix},\ \mathbf{J}_\mathrm{c} = \left[\mathbf{S}_\mathrm{a}\mathbf{M}^{-1}\mathbf{S}_\mathrm{p}\right]$$

and $\mathbf{S}_\mathrm{a}$, $\mathbf{S}_\mathrm{v}$ and $\mathbf{S}_\mathrm{d} \in \mathbb{R}^{n_\mathrm{d} \times n_\mathrm{DOF}}$ are selection matrices for acceleration, velocity and displacement, respectively, in which the locations of the measurements and/or difference relations can be specified.

For large civil engineering structures a model reduction is often performed, whereby the dynamics of the system is represented by a reduced number n_m of modal coordinates $\mathbf{z}(t) \in \mathbb{R}^{n_\mathrm{m}}$ as $\mathbf{u}(t) = \mathbf{\Phi}_\mathrm{r}\mathbf{z}(t)$, $\mathbf{\Phi}_\mathrm{r} \in \mathbb{R}^{n_\mathrm{DOF} \times n_\mathrm{m}}$. In state-space this corresponds to writing:

$$\mathbf{x}(t) = \begin{bmatrix} \mathbf{\Phi}_\mathrm{r} & \mathbf{0} \\ \mathbf{0} & \mathbf{\Phi}_\mathrm{r} \end{bmatrix} \boldsymbol{\zeta}(t)$$

where the modal state vector $\boldsymbol{\zeta}(t) \in \mathbb{R}^{2n_\mathrm{m}}$ now collects the modal coordinates:

$$\boldsymbol{\zeta}(t) = \begin{pmatrix} \mathbf{z}(t) \\ \dot{\mathbf{z}}(t) \end{pmatrix}.$$

The modal state-space model then becomes:

$$\dot{\boldsymbol{\zeta}}(t) = \mathbf{A}_\mathrm{c}\boldsymbol{\zeta}(t) + \mathbf{B}_\mathrm{c}\mathbf{p}(t) \tag{4}$$

$$\mathbf{d}(t) = \mathbf{G}_\mathrm{c}\boldsymbol{\zeta}(t) + \mathbf{J}_\mathrm{c}\mathbf{p}(t) \tag{5}$$

with the expressions for the reduced-order continuous-time system matrices $\mathbf{A}_\mathrm{c} \in \mathbb{R}^{2n_\mathrm{m} \times 2n_\mathrm{m}}$, $\mathbf{B}_\mathrm{c} \in \mathbb{R}^{2n_\mathrm{m} \times n_\mathrm{p}}$, $\mathbf{G}_\mathrm{c} \in \mathbb{R}^{n_\mathrm{d} \times 2n_\mathrm{m}}$ and $\mathbf{J}_\mathrm{c} \in \mathbb{R}^{n_\mathrm{d} \times n_\mathrm{p}}$ reducing to:

$$\mathbf{A}_\mathrm{c} = \begin{bmatrix} \mathbf{0} & \mathbf{I} \\ -\mathbf{\Omega}^2 & -\mathbf{\Gamma} \end{bmatrix} \tag{6}$$

$$\mathbf{B}_\mathrm{c} = \begin{bmatrix} \mathbf{0} \\ \mathbf{\Phi}^\mathrm{T}\mathbf{S}_\mathrm{p} \end{bmatrix} \tag{7}$$

$$\mathbf{G}_\mathrm{c} = \begin{bmatrix} \mathbf{S}_\mathrm{d}\mathbf{\Phi} - \mathbf{S}_\mathrm{a}\mathbf{\Phi}\mathbf{\Omega}^2 & \mathbf{S}_\mathrm{v}\mathbf{\Phi} - \mathbf{S}_\mathrm{a}\mathbf{\Phi}\mathbf{\Gamma} \end{bmatrix} \tag{8}$$

$$\mathbf{J}_\mathrm{c} = \left[\mathbf{S}_\mathrm{a}\mathbf{\Phi}\mathbf{\Phi}^\mathrm{T}\mathbf{S}_\mathrm{p}\right]. \tag{9}$$

Here $\mathbf{\Omega} = \text{diag}\{\omega_j\} \in \mathbb{R}^{n_m \times n_m}$ is a diagonal matrix containing the real eigenfrequencies ω_j in rad/s. The eigenvectors $\mathbf{\Phi}$ are assumed mass-normalized, which leads to the orthogonality conditions: $\mathbf{\Phi}^T\mathbf{M}\mathbf{\Phi} = \mathbf{I}$, and $\mathbf{\Phi}^T\mathbf{K}\mathbf{\Phi} = \mathbf{\Omega}^2$.

Proportional damping involves the assumption that the eigenvectors also diagonalize the damping matrix $\mathbf{C}$: $\mathbf{\Phi}^T\mathbf{C}\mathbf{\Phi} = \text{diag}\{2\xi_j\omega_j\} = \mathbf{\Gamma}$.

For the discretization of the full- or reduced-order state-space models – equations (2)&(3) or (4)&(5)) – a sampling rate of $1/\Delta t$ is used, with discrete time instants defined at $t_k = k\Delta t$ $(k = 1, \ldots, N)$. The discrete-time equivalent of the modal state-space model is then written as:

$$\mathbf{x}_{k+1} = \mathbf{A}\mathbf{x}_k + \mathbf{B}\mathbf{p}_k \tag{10}$$

$$\mathbf{d}_k = \mathbf{G}\mathbf{x}_k + \mathbf{J}\mathbf{p}_k \tag{11}$$

where $\mathbf{A} = e^{\mathbf{A}_c \Delta t}$, $\mathbf{B} = [\mathbf{A} - \mathbf{I}]\mathbf{A}_c^{-1}\mathbf{B}_c$, $\mathbf{G} = \mathbf{G}_c$, $\mathbf{J} = \mathbf{J}_c$, and the matrices $\mathbf{B}$ and $\mathbf{J}$ are converted from continuous to discrete time via a zero-order hold assumption (constant inter-sample behavior) on the input.

3. Coupled state and input estimation

In recent years various Kalman-type filters capable of jointly estimating the states $\mathbf{x}$ and input forces $\mathbf{p}$ based on a limited set of vibration measurements $\mathbf{d}$ have been suggested. A comparative study based on shake table experiments on a small-scale laboratory building was presented by Azam in 2015 [14]. This study involved three of the most commonly applied coupled input-state estimation algorithms, namely the joint input-state estimator (also sometimes referred to as the Gillijns & De Moor filter) [10, 11], the Augmented Kalman filter (AKF) [8], and the Dual Kalman filter (DKF) [9]. Recently also a 'smoothing' alternative was presented [12], where the input-state estimation is performed with a certain time delay.

The common basis for all these algorithms is the discrete-time state-space description (cf. previous section) supplemented with stochastic process and measurement noise $\boldsymbol{w}_k$ and $\boldsymbol{v}_k$:

$$\mathbf{x}_{k+1} = \mathbf{A}\mathbf{x}_k + \mathbf{B}\mathbf{p}_k + \boldsymbol{w}_k \tag{12}$$

$$\mathbf{d}_k = \mathbf{G}\mathbf{x}_k + \mathbf{J}\mathbf{p}_k + \boldsymbol{v}_k. \tag{13}$$

In the case of the AKF and DKF, the force evolution is also explicitly represented using a random walk model:

$$\mathbf{p}_{k+1} = \mathbf{p}_k + \boldsymbol{\eta}_k, \tag{14}$$

with $\boldsymbol{\eta}_k$ a component of the stochastic process $\{\boldsymbol{\eta}_k \in \mathbb{R}^{n_p}\}_{k=0}^{\infty}$. The addition of Eq. (14) allows for regularization of the inverse input estimation problem through an appropriate choice of the covariance matrix of the process $\boldsymbol{\eta}_k$.

3.1. Noise process assumptions

To arrive at the recursion formulae for all above mentioned coupled state-input estimators, certain assumptions on the noise processes $\{\boldsymbol{w}_k \in \mathbb{R}^{\mathrm{n_s}}\}_{k=0}^{\infty}$, $\{\boldsymbol{v}_k \in \mathbb{R}^{\mathrm{n_d}}\}_{k=0}^{\infty}$, (and $\{\boldsymbol{\eta}_k \in \mathbb{R}^{\mathrm{n_p}}\}_{k=0}^{\infty}$ in the case of the AKF/DKF) have to be made. Again a few common denominators can be formulated, namely that for all algorithms $\boldsymbol{w}_k$, $\boldsymbol{v}_k$, (and if applicable $\boldsymbol{\eta}_k$) are assumed to be zero-mean, white noise signals with known covariance matrices $\mathbf{Q} = \mathbb{E}\{\boldsymbol{w}_k \boldsymbol{w}_l^{\mathrm{T}}\} \geq \mathbf{0}$, $\mathbf{R} = \mathbb{E}\{\boldsymbol{v}_k \boldsymbol{v}_l^{\mathrm{T}}\} > \mathbf{0}$, (and $\mathbf{Q}^{\mathrm{p}} = \mathbb{E}\{\boldsymbol{\eta}_k \boldsymbol{\eta}_l^{\mathrm{T}}\} \geq \mathbf{0}$).

Depending on the specific formulation, the processes $\boldsymbol{w}_k$ and $\boldsymbol{v}_k$ are assumed to be mutually uncorrelated, or correlated in accordance with a predefined covariance matrix $\mathbf{S} = \mathbb{E}\{\boldsymbol{w}_k \boldsymbol{v}_l^{\mathrm{T}}\}$ (see for instance [15]). In general, however, the former assumption is made due to the absence of reliable information on the covariance matrix $\mathbf{S}$ in real life applications. In summary, the noise properties then amount to writing:

$$\mathbb{E}\left\{ \begin{bmatrix} \boldsymbol{w}_k \\ \boldsymbol{v}_k \end{bmatrix} \begin{bmatrix} \boldsymbol{w}_l^{\mathrm{T}} & \boldsymbol{v}_l^{\mathrm{T}} \end{bmatrix} \right\} = \begin{bmatrix} \mathbf{Q} & \mathbf{0} \\ \mathbf{0} & \mathbf{R} \end{bmatrix} \delta_{kl}. \tag{15}$$

As mentioned in the introduction the focus of this work is on having discrepancies between the theoretical assumptions made and the physical situation, as occuring in equivalent force based response monitoring, and the effect hereof on the estimation. The specific coupled input-state estimation algorithm used is therefore not of importance. A choice is made to generate the results used in the numerical examples of section 5 with the Gillijns & De Moor filter [10] due to its relative simplicity and the fact that the obtained results are independent of a third covariance matrix $\mathbf{Q}^{\mathrm{p}}$.

4. Response prediction using equivalent forces

Once the state and force estimates - $\hat{\mathbf{x}}$ and $\hat{\mathbf{p}}$ - have been obtained with a coupled input-state estimation algorithm, they can be used to estimate the full-field response of the structure. The idea was first presented in [11], and involves reformulating a new observation equation as follows:

$$\hat{\mathbf{d}}_{\mathrm{ex},k} = \mathbf{G}_{\mathrm{ex}} \hat{\mathbf{x}}_k + \mathbf{J}_{\mathrm{ex}} \hat{\mathbf{p}}_k \tag{16}$$

where $\hat{\square}$ denotes an estimated quantity, and the subscript $\square_{\mathrm{ex}}$ abbreviates extrapolated.

As mentioned already in the Introduction, the set of forces/force locations accounted for in $\hat{\mathbf{p}}/\mathbf{J}_{\mathrm{ex}}$ do not have to correspond to the true loading in situations where the main excitation sources are uncertain or time-varying. Instead, the force locations can be chosen with the soul aim of reproducing the full-field response $\hat{\mathbf{d}}_{\mathrm{ex},k}$. This latter case is referred to as equivalent force based response monitoring. It is stressed here that this is a powerful idea, since it potentially allows for real-time global response monitoring in the absence of any knowledge

of the driving forces, and using only a limited amount of sensors. Accordingly, the concept of equivalent force based response monitoring is being used more and more in various applications (cf. the Introduction), and sufficient clarity regarding the correct use of the concept in conjunction with a coupled input-state estimator is therefore becoming increasingly important.

When a set of equivalent forces $\hat{\mathbf{p}}$ is identified, the process and measurement noise $\boldsymbol{w}_k$ and $\boldsymbol{v}_k$ in Eq. (12) and (13) can be divided into contributions from force location errors, modelling errors, and sensor noise. For reduced-order systems constructed using Eq. (6) - (9), modelling errors consist of specifically eigenfrequency, eigenmode, and damping errors, i.e. errors on the dynamic properties. One can write:

$$\boldsymbol{w}_k = \{\boldsymbol{w}_k\}_{\text{force}} + \{\boldsymbol{w}_k\}_{\text{prop}} \tag{17}$$

$$\boldsymbol{v}_k = \{\boldsymbol{v}_k\}_{\text{force}} + \{\boldsymbol{v}_k\}_{\text{prop}} + \{\boldsymbol{v}_k\}_{\text{sensor}} \tag{18}$$

Defining $\square_{\text{real}}$ and $\square_{\text{eq}}$ as the matrices/vectors corresponding to respectively the real and equivalent force locations, the contributions from errors on these locations can be further specified as:

$$\{\boldsymbol{w}_k\}_{\text{force}} = \mathbf{B}_{\text{real}}\mathbf{p}_{k,\text{real}} - \mathbf{B}_{\text{eq}}\hat{\mathbf{p}}_k \tag{19}$$

$$\{\boldsymbol{v}_k\}_{\text{force}} = \mathbf{J}_{\text{real}}\mathbf{p}_{k,\text{real}} - \mathbf{J}_{\text{eq}}\hat{\mathbf{p}}_k \tag{20}$$

where $\mathbf{B}_{\text{eq}}$ and $\mathbf{J}_{\text{eq}}$ are constructed according to Eq. (7) and (9) using the assumed locations of the equivalent forces. Note that the two stochastic error processes become correlated in this case – $\mathbf{S} = \mathbb{E}\{\boldsymbol{w}_k\boldsymbol{v}_k^{\mathrm{T}}\} \neq \mathbf{0}$ – and depending on the nature of the excitation, are possibly no longer white. A more in-depth analysis of these error processes, including also the effects of intercorrelations between their individual elements, will be presented in the next section. To do so, first some additional notation is defined.

Recalling the definitions of the corresponding error covariance matrices $\mathbf{Q} = \mathbb{E}\{\boldsymbol{w}_k\boldsymbol{w}_l^{\mathrm{T}}\}$ and $\mathbf{R} = \mathbb{E}\{\boldsymbol{v}_k\boldsymbol{v}_l^{\mathrm{T}}\}$, and making a distinction between *real* and *assumed* covariances, one can write:

$$\mathbf{Q}_{\text{e}} = \mathbf{Q}_{\text{real}} - \mathbf{Q}_{\text{as}} \tag{21}$$

$$\mathbf{R}_{\text{e}} = \mathbf{R}_{\text{real}} - \mathbf{R}_{\text{as}} \tag{22}$$

$$\mathbf{S}_{\text{e}} = \mathbf{S}_{\text{real}} - \mathbf{S}_{\text{as}} \tag{23}$$

where the subscripts 'e' and 'as' denote erroneous and assumed, respectively, and the real covariances are those specified in equations (17) and (18). These matrices can be further decomposed into blocks representing (in the case of a modally reduced state-space representation) the (co)variances between the modal displacements $\mathbf{z}$, the modal velocities $\dot{\mathbf{z}}$, and the data $\mathbf{d}$, respectively:

$$\mathbf{Q}_{\mathrm{e}} = \begin{bmatrix} \mathbf{Q}_{\mathrm{e},\mathbf{zz}} & \mathbf{Q}_{\mathrm{e},\mathbf{z\dot{z}}} \\ \mathbf{Q}_{\mathrm{e},\mathbf{\dot{z}z}} & \mathbf{Q}_{\mathrm{e},\mathbf{\dot{z}\dot{z}}} \end{bmatrix}; \quad \mathbf{S}_{\mathrm{e}} = \begin{bmatrix} \mathbf{S}_{\mathrm{e},\mathbf{zd}} \\ \mathbf{S}_{\mathrm{e},\mathbf{\dot{z}d}} \end{bmatrix} \tag{24}$$

where $\mathbf{Q}_{\mathrm{e},\mathbf{zz}}$, $\mathbf{Q}_{\mathrm{e},\mathbf{z\dot{z}}}$, $\mathbf{Q}_{\mathrm{e},\mathbf{\dot{z}\dot{z}}} \in \mathbb{R}^{(\mathrm{n_s}/2)\times(\mathrm{n_s}/2)}$ and $\mathbf{S}_{\mathrm{e},\mathbf{zd}}$, $\mathbf{S}_{\mathrm{e},\mathbf{\dot{z}d}} \in \mathbb{R}^{(\mathrm{n_s}/2)\times n_{\mathrm{d}}}$.

5. Numerical examples

A 21-node cantilever beam model is constructed based on Euler-Bernoulli beam theory and subsequently reduced to 10 degrees of freedom on the basis of the first 10 modes. The properties of the beam are as presented in Table 1. The first three natural frequencies of the beam are 0.56, 3.51, and 9.82 Hz, respectively. The calculated modal properties are subsequently used to construct a reduced-order modal state-space model using equations (6) - (9), where a modal damping ratio of 2% is assumed for all modes. A graphical representation of the beam including the sensor networks used in the upcoming examples are shown in Fig. 1.

Table 1: Beam properties

Length	L	1	[m]
Structural mass	m	1	[kg/m]
Flexural rigidity	EI	1	[Nm^2]
Damping ratio	ζ	0.02	[−]

The excitation, applied at the tip of the cantilever, is chosen as a superposition of two harmonic forces with frequencies equal to 2.03 Hz and 6.66 Hz, respectively. These frequencies are chosen as the average of respectively the first and second, and second and third, natural frequency of the structure. A sampling frequency of 1000 Hz is used in all the following examples, satisfying the Nyquist-Shannon sampling criterion with respect to the highest load frequency and all structural frequencies up to the 6th mode. It is mentioned that when the coupled input-state estimation is performed based on real data, the selected time step size should also be chosen with regard to the physical delay in the system, in order to ensure that causality is respected [16, 17].

An overview of the cases that will be analyzed in the following sections is presented in Table 2. It is important to note that, for all cases, the data sets used and chosen (equivalent) force locations *satisfy the observability, controllability, direct invertibility, and stability criteria* as formulated in [13].

To analyze the effect of specifically the equivalent force assumptions, no modelling errors will be included during the analyses, implying that $\{\boldsymbol{w}_k\}_{\mathrm{prop}} = \{\boldsymbol{v}_k\}_{\mathrm{prop}} = 0$ in equations (17) and (18), whereby the error processes reduce to $\boldsymbol{w}_k = \{\boldsymbol{w}_k\}_{\mathrm{force}}$ and $\boldsymbol{v}_k = \{\boldsymbol{v}_k\}_{\mathrm{force}} + \{\boldsymbol{v}_k\}_{\mathrm{sensor}}$. Also the sensor noise levels are chosen to be negligible. Each measurement signal is corrupted with a white noise signal whose standard deviation is proportional to the standard deviation of the measurement signal itself. The measurement noise of the i^{th} sensor is

Table 2: Overview of cases analyzed.

Section:	*Case:*	*Eqv. load type:*	*Location:*
5.2	Load at the tip	nodal	3L/4
5.3			L/4
5.4			L/4, L/2, 3L/4, L
5.5		modal	$\mathbf{\Phi}_1, \mathbf{\Phi}_2, \mathbf{\Phi}_3, \mathbf{\Phi}_4$
5.6	Moving load	modal	$\mathbf{\Phi}_1, \mathbf{\Phi}_2, \mathbf{\Phi}_3, \mathbf{\Phi}_4$

modelled as: $\{\boldsymbol{v}\}^i_{\text{sensor}} = \xi\sigma_{\mathbf{d}_i}\mathbf{r}$, with $\xi = 1\text{e}{-12}$ the fixed low noise level, $\sigma_{\mathbf{d}_i}$ the standard deviation of the considered output, and $\mathbf{r} \in \mathbb{R}^{\text{N}}$ a vector of random values drawn independently from a normal distribution with zero mean and unit standard deviation.

The assumed noise matrix $\mathbf{R}_{\text{as}}$ is consistent with the added sensor noise, so that $\mathbf{R}_{\text{e}}$ of equation (22) is related solely to the force positions: $\mathbf{R}_{\text{e}} = \mathbb{E}\left\{\{\boldsymbol{v}_k\}_{\text{force}}\{\boldsymbol{v}_k\}^{\text{T}}_{\text{force}}\right\}$. By also assuming $\mathbf{Q}_{\text{as}} = \mathbf{0}$ and $\mathbf{S}_{\text{as}} = \mathbf{0}$ in the following sections, $\mathbf{Q}_{\text{e}}$ and $\mathbf{S}_{\text{e}}$ can be similarly related solely to the force positions: $\mathbf{Q}_{\text{e}} = \mathbb{E}\left\{\{\boldsymbol{w}_k\}_{\text{force}}\{\boldsymbol{w}_k\}^{\text{T}}_{\text{force}}\right\}$ and $\mathbf{S}_{\text{e}} = \mathbb{E}\left\{\{\boldsymbol{w}_k\}_{\text{force}}\{\boldsymbol{v}_k\}^{\text{T}}_{\text{force}}\right\}$ – cf. equations (19) and (20).

In order to rule out any effects on the results of potential initialization errors or different convergence speeds, the first 10 seconds of each data trace will be neglected during the post processing.

5.1. Collocated nodal force

First a situation is considered where the force location is known exactly, and no use is made of the concept of equivalent forces: $\{\boldsymbol{w}_k\}_{\text{force}} = \{\boldsymbol{v}_k\}_{\text{force}} = 0$, and consequently $\mathbf{Q}_{\text{e}} = \mathbf{R}_{\text{e}} = \mathbf{S}_{\text{e}} = \mathbf{0}$. The nodal force applied at the tip of beam is identified in conjunction with the 10 modal states. Simulated data from 4 accelerometers and 1 strain gauge is used for the estimation, as shown in Fig. 1a.

As expected, all modal states and the force are identified with high accuracy, allowing for an error-free extrapolation of the response of the beam to any location by means of Eq. 16. Results are omitted.

5.2. Nodal equivalent force at 3L/4

For the next analysis an equivalent force is considered to act at $3L/4$, representing a situation where only some uncertain information on the force location is available. In this case $\{\boldsymbol{w}_k\}_{\text{force}} \neq 0$ and $\{\boldsymbol{v}_k\}_{\text{force}} \neq 0$, and consequently all error matrices – $\mathbf{Q}_{\text{e}}$, $\mathbf{R}_{\text{e}}$, and $\mathbf{S}_{\text{e}}$ – will become populated. The force-state estimation is performed based on the same measurement set as before.

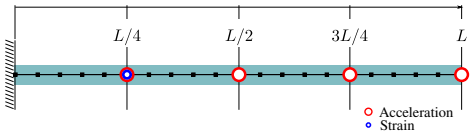

(a)

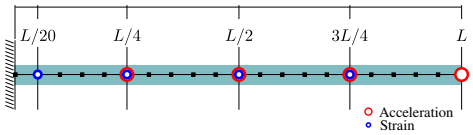

(b)

Figure 1: Analyzed beam including sensor networks a) with one strain measurement, and b) with four strain measurements.

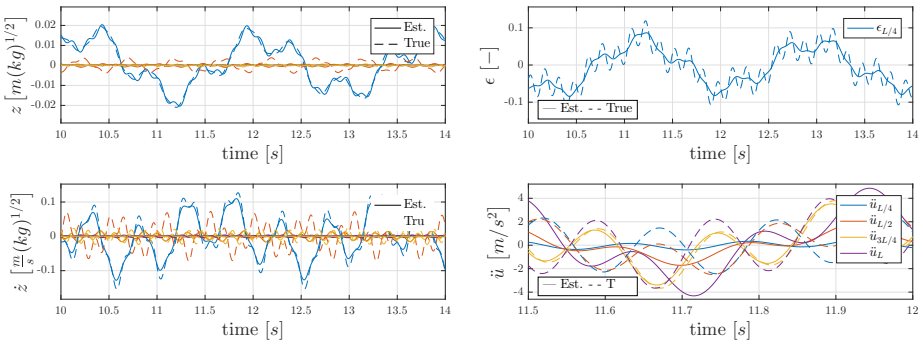

(a) (b)

Figure 2: True (dashed lines) and estimated (solid lines) time histories of (a) the modal states and (b) the predicted strain and accelerations. Nodal equivalent force at 3L/4.

State, i:	1	2	3	4	5
$RMS_{z,i}$	5.02e-02	6.79e-01	7.49e-01	9.49e-01	6.90e-01
State, i:	6	7	8	9	10
$RMS_{z,i}$	3.29e-01	2.91e-01	2.38e-01	2.98e-01	7.27e-01

Table 3: RMS values of normalized state estimate error. Nodal equivalent force at 3L/4.

Fig. 2 shows, on the left, the true and estimated modal states (top) and modal velocities (bottom) for the first 3 modes. Although the first modal displacement is identified relatively accurately, the discrepancies between the simulated and estimated modal states become larger for the higher modes. To quantify these errors an RMS error measure for each modal state is defined as follows:

$$\mathrm{RMS}_{z,i} = \sqrt{\frac{1}{\mathrm{N}} \sum_{k=1}^{\mathrm{N}} \left(\frac{z_k^i - \hat{z}_k^i}{\max|z^i|} \right)^2} \tag{25}$$

where i is the mode number. To disregard the effect on the error of having large differences in orders of magnitude between the different states, the simulated states are first normalized to unity and the corresponding scale factors subsequently used to scale also the estimates. The difference between the scaled versions of the simulated and estimated state is finally used to compute the normalized RMS error defined in Eq. 25. Table 3 presents these values for the modal displacements in the current problem, clearly showing an increased error for the higher-order modes, with a maximum occurring in mode 4.

Fig. 2 and Table 3 show that the modal states and forces cannot be reconstructed uniquely, an effect caused by a violation of various assumptions used in the derivation of the estimator. Since the identified modal estimates are incorrect, the data reconstructed on the basis of these estimates – see equation (16) – will also be incorrect, as shown on the right in Fig. 2. Note that here we are not even attempting to reconstruct at locations other than those measured, and still there exists a clear discrepancy between measured and reconstructed data.

To further analyze these effects, Fig. 3 shows examples of realizations (time traces) for various covariances that can be used to construct the error matrices $\mathbf{Q}_\mathrm{e}$, $\mathbf{R}_\mathrm{e}$, and $\mathbf{S}_\mathrm{e}$. Fig. 3a shows, for instance, the time traces corresponding to all entries of the matrix $\{\boldsymbol{w}_{k,\mathbf{z}} \boldsymbol{w}_{k,\mathbf{z}}^\mathrm{T}\}_{k=0}^\mathrm{N} \in \mathbb{R}^{(\mathrm{n_s}/2)\times(\mathrm{n_s}/2)}$, where $\boldsymbol{w}_{k,\mathbf{z}} \in \mathbb{R}^{\mathrm{n_s}/2}$ collects only those components of $\boldsymbol{w}_k$ corresponding to the modal displacements $\mathbf{z}$. The average of each of these time traces thus corresponds to an element of the matrix $\mathbf{Q}_{\mathrm{e},\mathbf{zz}}$ as defined in equation (24). Recall that in the current study realizations of all these components of the process and measurement noise $\{\boldsymbol{w}_k \in \mathbb{R}^{\mathrm{n_s}}\}_{k=0}^\mathrm{N}$ and $\{\boldsymbol{v}_k \in \mathbb{R}^{\mathrm{n_d}}\}_{k=0}^\mathrm{N}$ can be calculated using equations (19) and (20).

The frequency content of the realizations in Fig. 3 can be related to that of the true and estimated forces, plotted in Fig. 4. The frequency of the two

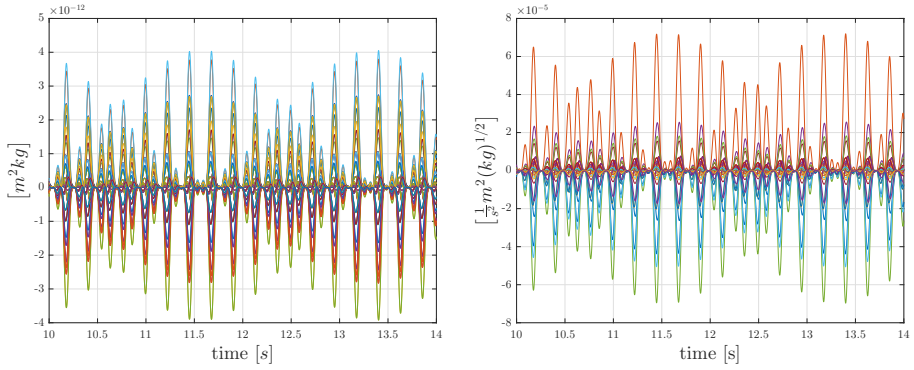

(a) (b)

Figure 3: Time traces used to calculate all entries of a) $\mathbf{Q}_{\mathrm{e},\mathbf{zz}} \in \mathbb{R}^{(\mathrm{n_s}/2)\times(\mathrm{n_s}/2)}$ and (b) $\mathbf{S}_{\mathrm{e},\mathbf{zd}} \in \mathbb{R}^{(\mathrm{n_s}/2)\times n_\mathrm{d}}$ for the case of a nodal equivalent force at 3L/4.

harmonics in the latter figure are in fact doubled in the error realizations due to the fact that these are based on the square of the errors $\left(\sin^2(x) = \frac{1-\cos(2x)}{2}\right)$. It is also worth noting that the error traces in Fig. 3 are *not* white noises, as is the assumption in the filter. The effect hereof on the optimality of the estimates is considered outside the scope of this work. Due to the fact that the applied loading is a zero-mean harmonic force, no unaccounted for bias errors are, however, introduced. Also here it is worth noting, though, that having bias violations in the case of non-zero applied forces will cause additional errors not analyzed in the examples presented in this contribution.

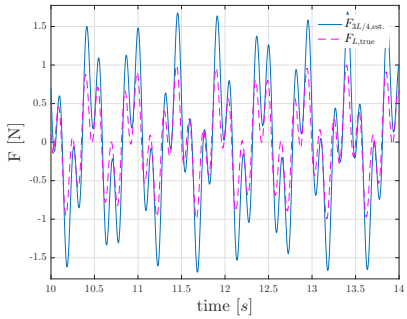

(a)

Figure 4: True (dashed lines) and estimated (solid lines) time histories of nodal force at L and 3L/4 respectively.

To analyze further the effect on the estimates of assuming an erroneous force location, the mean of all error realizations, i.e. the matrices $\mathbf{Q}_{\mathrm{e},\mathbf{zz}}$, $\mathbf{Q}_{\mathrm{e},\mathbf{z\dot{z}}}$, $\mathbf{S}_{\mathrm{e},\mathbf{zd}}$, and $\mathbf{R}_\mathrm{e}$, defined in Eq. 24, are plotted in Fig. 5. Of these matrices, particularly

State, i:	1	2	3	4	5
$RMS_{z,i}$	3.06e+00	2.97e+00	3.05e+00	4.04e+00	1.72e+00
State, i:	6	7	8	9	10
$RMS_{z,i}$	1.59e+00	4.05e+00	3.92e+00	1.78e+00	1.78e+00

Table 4: RMS values of normalized state estimate error. Nodal equivalent force at L/4.

interesting to consider are $\mathbf{Q}_{\mathrm{e},\mathbf{zz}}$ (or $\mathbf{Q}_{\mathrm{e},\mathbf{z\dot{z}}}$) and $\mathbf{S}_{\mathrm{e},\mathbf{zd}}$, since they can most easily be related to the uniqueness of the modal state estimates on the one side, and the uniqueness of the coupled input-state estimates on the other.

It is clear from the nonzero off-diagonal elements in $\mathbf{Q}_{\mathrm{e},\mathbf{zz}}$ in Fig. 5a that the force error correlates the state errors, especially between modal displacements 2, 3, 4, 5 and 10. Note that the effect hereof is clearly visible in the results presented in Table 3, where the largest error was found in modal state 4, corresponding to the location of the largest entry on the diagonal of $\mathbf{Q}_{\mathrm{e},\mathbf{zz}}$ in Fig. 5. The same observation can be made with regard to the error covariances between the modal displacements and velocities shown in Fig. 5b. Due to these unaccounted-for correlations, the algorithm is not able to uniquely identify the states.

Similar conclusions can be drawn with regard to the uniqueness of the state versus force estimates on the basis of the matrix $\mathbf{S}_{\mathrm{e},\mathbf{zd}}$ in Fig. 5c. The force error strongly correlates the state error on for instance modal displacement 4 with the measurement error on the tip acceleration, implying that it will be difficult to distinguish between (and thus uniquely identify) the force and modal state 4 on the basis of this measurement.

As concerns Fig. 5d, the correlations between acceleration errors at L and $3L/4$ are seen to be the largest, which can easily be explained by realizing that these are the positions used to construct the direct transmission terms in equation (20).

A final note is made on Fig. 5c and 5d: the direct transmission terms in Eq. 13 do not influence strain outputs since all corresponding entries in $\mathbf{S}_a$ are zero, and thus all error covariance terms related to strain outputs are zero (denoted by a dot in the figure).

5.3. Nodal equivalent force at L/4

Next a case is considered in which the equivalent force is located at $L/4$ from the support, while the true applied force is still acting at L. The measurement set remains unchanged, and all observability, controllability, direct invertibility, as well as stability criteria remain satisfied. As expected, the accuracy of the state estimates drastically decreases, as shown in Fig. 6a and Table 4. The response prediction consequentially deteriorates as well, as shown in Fig. 6b.

Compared to excitation at L, the placement of an equivalent force at $L/4$ correlates more modal errors – see matrix $\mathbf{Q}_{\mathrm{e},\mathbf{zz}}$ in Fig. 7. (Note that the matrices $\mathbf{Q}_{\mathrm{e},\mathbf{z\dot{z}}}$ and $\mathbf{R}_{\mathrm{e}}$ have been and will from now on be omitted from these figures since they do not add any valuable information). The correlations in

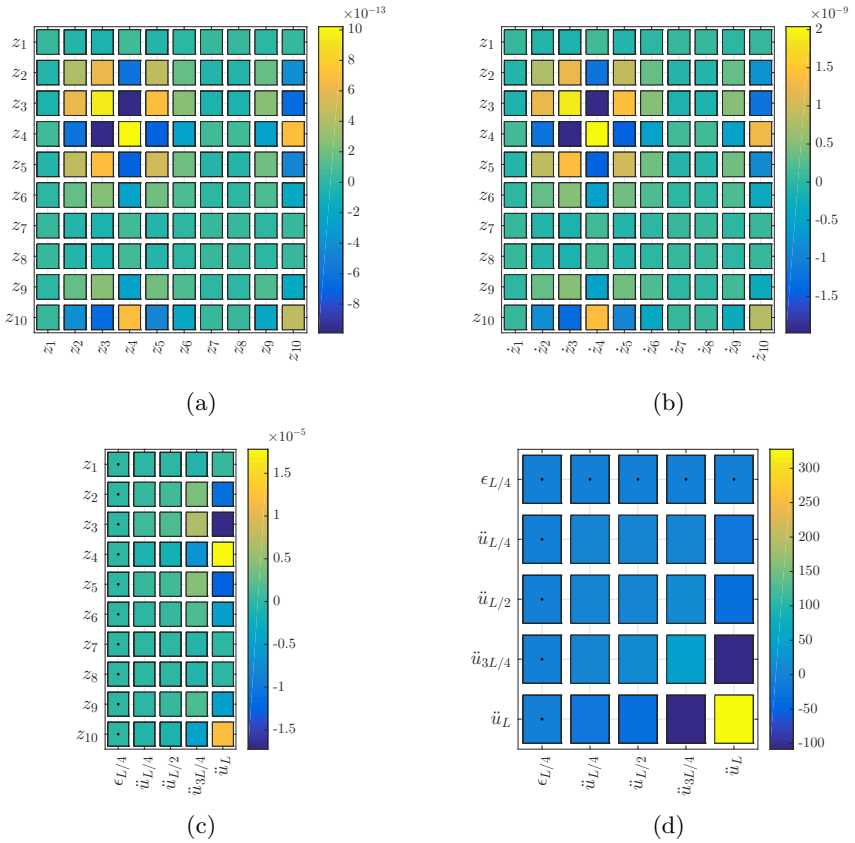

Figure 5: Error covariance matrices (a) $\mathbf{Q}_{\mathrm{e},\mathbf{zz}}$, (b) $\mathbf{Q}_{\mathrm{e},\mathbf{z\dot{z}}}$, (c) $\mathbf{S}_{\mathrm{e},\mathbf{zd}}$, and (d) $\mathbf{R}_{\mathrm{e}}$. Nodal equivalent force at 3L/4.

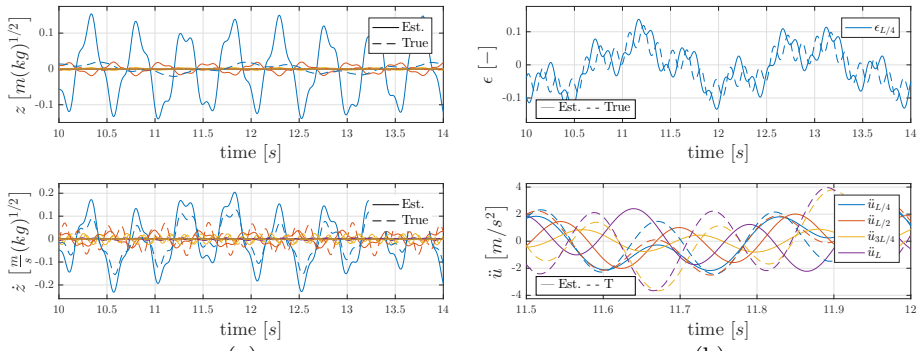

Figure 6: True (dashed lines) and estimated (solid lines) time histories of (a) the modal states and (b) the predicted strain and accelerations. Nodal equivalent force at L/4.

$\mathbf{Q}_{\mathrm{e},\mathbf{zz}}$ are also much stronger, as can be concluded from the order of magnitude of its components compared to those in Fig. 5a. The normalized RMS state errors are also an order of magnitude larger – cf. Table 3 and 4.

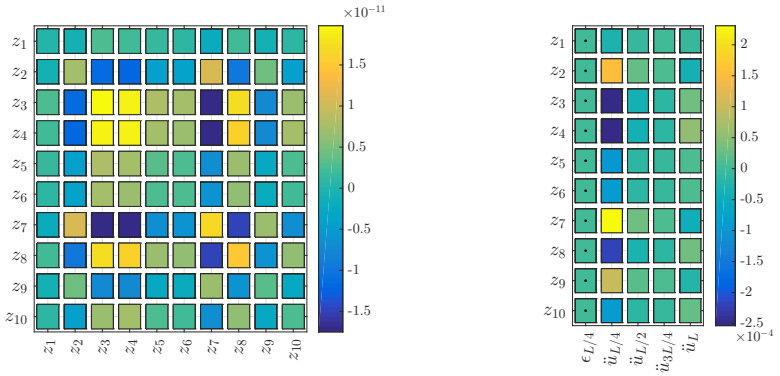

(a) (b)

Figure 7: Error covariance matrices (a) $\mathbf{Q}_{\mathrm{e},\mathbf{zz}}$ and (b) $\mathbf{S}_{\mathrm{e},\mathbf{zd}}$. Nodal equivalent force at L/4.

From the stronger correlations in $\mathbf{S}_{\mathrm{e},\mathbf{zd}}$ in Fig. 7b it can also be concluded that with an increased force error it becomes increasingly difficult to distinguish between the effects of the force and those of the states on the measurements.

5.4. Equivalent forces at sensor locations

The case where equivalent forces are assumed to act at the sensor locations is often seen – see e.g. [18, 11] – because it leads to a well-conditioned direct transmission matrix $\mathbf{J}$. The typical ill-conditioning of the input estimation resulting from non-collocation is thus avoided.

For the current problem this case implies having equivalent forces at L/4, L/2, 3L/4 and L. Since the number of forces to be identified has now increased, it is necessary to revise the direct invertibility and stability requirements [13]. In order to ensure a stable system inversion, it becomes necessary to measure at least three additional displacements/strains. A new sensor network is thus defined as illustrated in Fig. 1b. This new network also satisfies all additional criteria related to observability and controllability. Response estimation results are shown in Fig. 8.

The modal displacements and velocities are seen to be estimated with high accuracy in Fig. 8a, allowing for accurate response predictions at the sensor locations (Fig. 8b) as well as at all other unmeasured locations. This high accuracy can be attributed to having neglible discrepancies between the real and assumed error covariance matrices, as illustrated in Fig. 9, where the error magnitudes are of the order e^{-38} and e^{-31} on the matrices $\mathbf{Q}_{\mathrm{e},\mathbf{zz}}$ and $\mathbf{S}_{\mathrm{e},\mathbf{zd}}$, respectively.

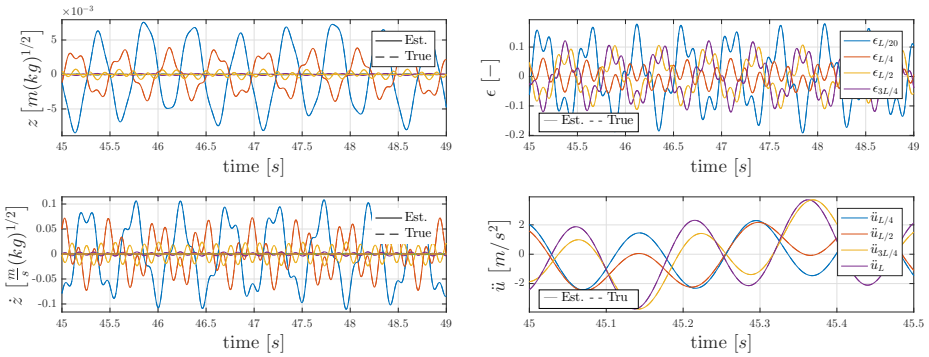

Figure 8: True (dashed lines) and estimated (solid lines) time histories of (a) the modal states and (b) the predicted strains and accelerations. Equivalent forces at sensor locations.

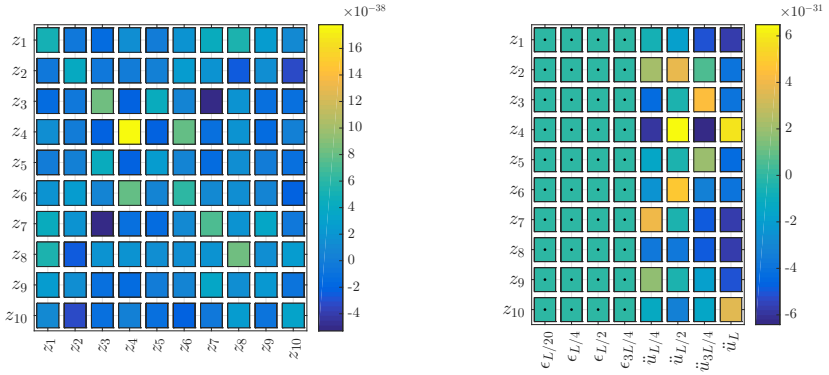

Figure 9: Error covariance matrices (a) $\mathbf{Q}_{\mathrm{e},\mathbf{zz}}$ and (b) $\mathbf{S}_{\mathrm{e},\mathbf{zd}}$. Equivalent forces at all sensor locations.

It is important to realize, though, that it cannot be concluded that identifying equivalent forces at the sensor locations will in general lead to accurate response estimations. Considering again equations (19) and (20), it can be deduced that $\{\boldsymbol{w}_k\}_{\text{force}}$ and $\{\boldsymbol{v}_k\}_{\text{force}}$ and therefore the response estimation error will depend on a) whether a sensor/equivalent force is placed at the exact force location(s), and b) the difference between the norm of the column(s) of $\mathbf{B}_{\text{eq}}$ and $\mathbf{J}_{\text{eq}}$ corresponding to the true force location(s) and the norm of their other columns. The smaller the difference, the larger the response estimation error will be, since the amplitudes of the identified forces at the true as opposed to the other equivalent force locations will become comparable. The current example, where the true force is acting at the most sensitive location of the beam (the tip), can in this sense be viewed as an ideal case, since the norms of the matrices $\mathbf{B}_{\text{eq}}$ and $\mathbf{J}_{\text{eq}}$ will be significantly larger at this location than at L/4, L/2, and 3L/4. The error made through the addition of the other equivalent forces is thus relatively small and the reconstruction is good. RMS values of the normalized state estimation errors as defined in Eq. 25 is of the order of magnitude e^{-13} (cf. tables 3 and 4 for previous results).

5.5. Modal equivalent forces

A simple way to ensure that the states can be related to the forces in a unique way, is the identification of modal equivalent forces. For a system consisting of n_{m} modes and n_{p} modal forces, this is achieved by defining:

$$\boldsymbol{\Phi}^{\text{T}}\mathbf{S}_{\text{p}} = \begin{bmatrix}\mathbf{I}_{n_{\text{p}}\times n_{\text{p}}} & \mathbf{0}_{n_{\text{p}}\times(n_{\text{m}}-n_{\text{p}})}\end{bmatrix}^{\text{T}} \tag{26}$$

and then proceeding to construct $\mathbf{B}_{\text{c}}$, $\mathbf{J}_{\text{c}}$, $\mathbf{B}$ and $\mathbf{J}$ as in equations (7) and (9). Apart from ensuring a unique force-state relation, modal forces can be used for response prediction in applications where the spatial force distributions are complex or time-varying, making it difficult to explicitly define $\mathbf{S}_{\text{p}}$. Examples here are aerodynamic or hydrodynamic loading.

Correctly choosing the modal forces is crucial for an accurate response prediction, since the chosen modes must be able to represent the (dynamic and static) response of the structure. Two conflicting requirements arise in this regard: on the one side a sufficient number of modal forces is required in order to assure an accurate response prediction over a possibly broad range of frequencies and operational deflection shapes, whereas the number of equivalent modal forces is simultaneously restricted by the number of acceleration and displacement/strain measurements through the direct invertibility and stability criteria [13].

Recall that in the current example, the excitation frequencies of the beam are chosen as the average of respectively the first and second, and second and third, natural frequency of the structure. A choice is made to identify four modal forces in order to drive the modal response of the first four modes. This allows for the use of the same sensor network as in the previous section - cf. Fig. 1b. Results are presented in Fig. 10 and 11.

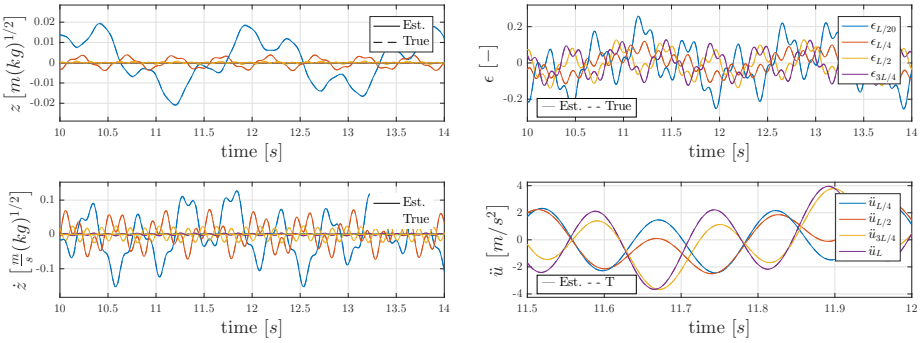

Figure 10: True (dashed lines) and estimated (solid lines) time histories of (a) the modal states and (b) the predicted strains and accelerations. Modal equivalent forces.

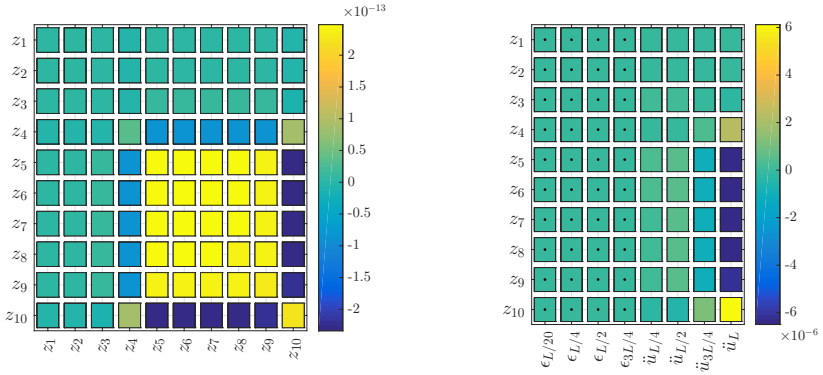

Figure 11: Error covariance matrices (a) $\mathbf{Q}_{\mathrm{e},\mathbf{zz}}$ and (b) $\mathbf{S}_{\mathrm{e},\mathbf{zd}}$. Modal equivalent forces.

State, i:	1	2	3	4	5
$RMS_{z,i}$	6.56e-03	8.97e-03	2.04e-02	1.75e-01	5.00e-01
State, i:	6	7	8	9	10
$RMS_{z,i}$	4.99e-01	4.99e-01	4.99e-01	4.99e-01	4.99e-01

Table 5: RMS values of normalized state estimate error. Modal equivalent forces.

As expected, the modal states and velocities are again identified with high accuracy in Fig. 10, which would allow for an equally accurate extrapolation of the measured data to unmeasured locations. This is possible since the unaccounted-for couplings in the error covariances matrices (e.g. $\mathbf{Q}_{\mathrm{e},\mathbf{zz}}$ and $\mathbf{S}_{\mathrm{e},\mathbf{zd}}$) are now restricted to modes that hardly contribute to the response, as shown in Fig. 11. The RMS values of the normalised state estimation errors are shown in Table 5, where the error on the (first) modal state most dominant in the response is seen to be at least one order of magnitude smaller than with nodal equivalent forces at 3L/4 or L/4.

In contrast to identifying response-driving equivalent forces at the sensor locations (section 5.4), the strategy of identifying equivalent modal forces will allow for accurate response extrapolation in *any* type of structure excited by forces at *any* possible location(s), on the condition that the modes included in the modal force selection are able to fully represent the response of the structure to the applied loading. It should be noted that for structures with rich dynamics this could possibly imply the inclusion of a large number of modal forces, which in turn would require a very extensive sensor network, in order to satisfy the direct invertibility and stability criteria. In practice, though, it is possible to partly bypass this effect by including displacement measurements calculated by (offline) numerical integration of the measured accelerations – see e.g. [2]. A quantification of the error introduced by the integration in these cases, and the effect thereof on the response estimates, is considered outside the scope of the current investigation.

5.6. The moving load problem

In this final example the moving load problem is considered, mainly due to its relevance in the fatigue monitoring of bridges excited by moving traffic. Note that in contrast to the previous section, it is not the type/location(s) of the equivalent force(s) that are changing in this example, but the applied loading itself. Response signals are generated for the sensor network defined in Fig. 1b, but now due to a point load moving at a velocity of $1/T_4$ m/s, where $T_4 = \pm 0.05s$ is the fourth natural period of the beam. Drawing on the insights gained in the previous sections on the importance of unique state-force relations, a set of four modal equivalent forces are identified in order to drive the response. Results are presented in Fig. 12.

As expected and partly also shown in Fig. 12a, the moving point load draws response from various modes of the beam. The use of four modal forces is in

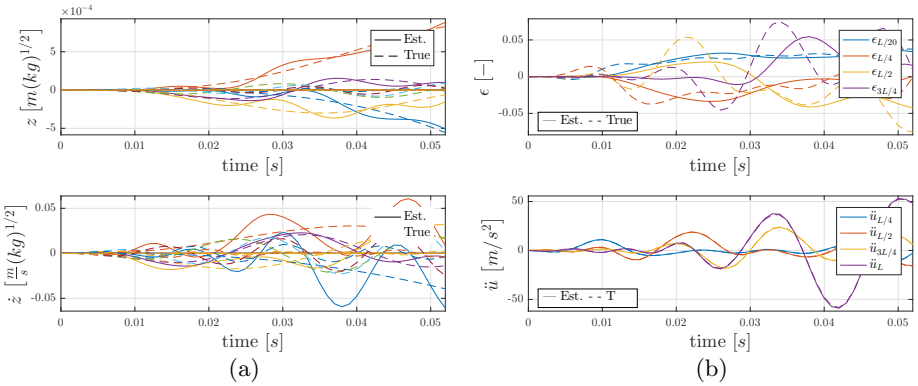

Figure 12: True (dashed lines) and estimated (solid lines) time histories of (a) the modal states and (b) the predicted strain and accelerations. Moving load case with four modal equivalent loads.

this case not sufficient, and leads to inaccurate modal displacement and velocity estimates. The response prediction errors shown in Fig. 12b are seen to be significantly higher for the strains as opposed to the accelerations, which is most likely due to the differences in their order of magnitudes.

Fig. 13 shows the modal loads themselves, calculated and identified as $\mathbf{\Phi}^{\mathrm{T}}\mathbf{S}_{\mathrm{p}}\mathbf{p}(t)$ on the basis of Eq. 26, but with the force allocation matrix $\mathbf{S}_{\mathrm{p}}(t)$ now time dependent. As with the states presented in Fig. 12a, large discrepancies exist between the true and identified modal forces. The reconstructed accelerations at the measurement locations (Fig. 12b) are, however, matched rather accurately. This again points to a problem of non-uniqueness in the solution, which in this case stems from the fact that there are not enough sensors/modal forces to account for the higher number of modes contributing to the response of the beam to the moving load. It is thus not possible to sufficiently constrain the inverse solution to produce state-force estimates that would accurately predict the response also at locations other than those measured. Note that it is in this case not meaningful to view the error covariance matrices $\mathbf{Q}_{\mathrm{e},\mathbf{zz}}$ and $\mathbf{S}_{\mathrm{e},\mathbf{zd}}$, due to the transient nature of the loading/response.

6. Conclusions

Modal state and force estimates obtained with Kalman-type filters can be used to estimate the full-field response of a structure from sparse vibration measurements. In this contribution, the focus was on situations where no knowledge on the applied loading is available, neither in terms of its dynamic content, nor its spatial distribution, and response-driving equivalent forces are identified. It was shown that, unlike commonly assumed, the success of this type of equivalent force based response monitoring cannot be related solely to whether the chosen set of equivalent forces satisfy the controllability requirements. Since modal states that are *simultaneously* excited by the equivalent forces cannot be

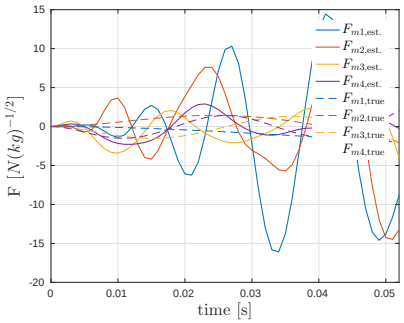

(a)

Figure 13: True (dashed lines) and estimated (solid lines) time histories of the first four modal forces.

uniquely identified if the assumed position of the force is wrong, results remain sensitive to a correct assumptions on the force locations. This is mainly due to the fact that no correlation is assumed between the noise processes on the individual elements of respectively the process and measurement noise (both $\mathbf{Q}$ and $\mathbf{R}$ are assumed diagonal), whereas these correlations in fact increase with the distance between the positions of the equivalent and applied loads.

The identification of modal equivalent forces can solve this problem, since the correlations are then dissolved, but require at least one acceleration and displacement/strain sensor for every mode excited, making it practically feasible only for systems exhibiting relatively low-order or band limited dynamic behavior. Examples of such structures for which also the final goal of fatigue monitoring could be of interest are the supporting structures for offshore wind turbines, wind-excited tall buildings, or structures driven mainly by periodic loads, whereas the applicability to for instance slender bridges excited by moving loads will in general be limited, depending on the number of modes that is excited. The latter will in turn depend on the dynamic properties of the bridge, its unevenness, the contact area of the tyres, etc.

It is finally mentioned that all conclusions drawn pertain only to forced vibration systems, and is of no concern for systems excited mainly by transient loads.

Acknowledgements

The research presented in this paper was performed within the framework of the project “EUROS: Excellence in Uncertainty Reduction for Offshore wind Systems”, which is supported by the Dutch Technology Foundation STW, a component of the Netherlands Organisation for Scientific Research (NWO), partly funded by the Ministry of Economic Affairs. Their financial support is gratefully acknowledged.

References

[1] C. Papadimitriou, C.-P. Fritzen, P. Kraemer, and E. Ntotsios. Fatigue predictions in entire body of metallic structures from a limited number of vibration sensors using Kalman filtering. 2011. Published online in Wiley InterScience (www.interscience.wiley.com). DOI:10.1002/stc.395.

[2] Kristof Maes, A Iliopoulos, W Weijtjens, C Devriendt, and Geert Lombaert. Dynamic strain estimation for fatigue assessment of an offshore monopile wind turbine using filtering and modal expansion algorithms. *Mechanical Systems and Signal Processing*, 76:592–611, 2016.

[3] V. Dertimanis, E. Chatzi, S.E. Azam, and C. Papadimitriou. Output-only fatigue prediction of uncertain steel structures. In *8th European Workshop On Structural Health Monitoring (EWSHM 2016), Bilbao, Spain*, 2016.

[4] T. S. Nord, E. Lourens, M. Määttänen, O. Øiseth, and K.V. Høyland. Laboratory experiments to study ice-induced vibrations of scaled model structures during their interaction with level ice at different ice velocities. *Cold Regions Science and Technology*, 119:1–15, 2015.

[5] T.S. Nord, O. Øiseth, and E. Lourens. Ice force identification on the Norströmsgrund lighthouse. *Computers & Structures*, 169:24–39, 2016.

[6] A. Iliopoulos, R. Shirzadeh, W. Weijtjens, P. Guillaume, D. Van Hemelrijck, and C. Devriendt. A modal decomposition and expansion approach for prediction of dynamic responses on a monopile offshore wind turbine using a limited number of vibration sensors. *Mechanical Systems and Signal Processing*, 68:84–104, 2016.

[7] A. Iliopoulos, W. Weijtjens, D. Van Hemelrijck, and C. Devriendt. Fatigue assessment of offshore wind turbines on monopile foundations using multi-band modal expansion. *Wind Energy*, 2017.

[8] E Lourens, E. Reynders, G. De Roeck, G. Degrande, and G. Lombaert. An augmented kalman filter for force identification in structural dynamics. *Mechanical Systems and Signal Processing*, 27:446–460, 2012.

[9] S.Ẽ. Azam, E. Chatzi, and C. Papadimitriou. A dual kalman filter approach for state estimation via output-only acceleration measurements. *Mechanical Systems and Signal Processing*, 60:866–886, 2015.

[10] S. Gillijns and B. De Moor. Unbiased minimum-variance input and state estimation for linear discrete-time systems with direct feedthrough. 43(5):934–937, 2007.

[11] E. Lourens, C. Papadimitriou, S. Gillijns, E. Reynders, G. De Roeck, and G. Lombaert. Joint input-response estimation for structural systems based on reduced-order models and vibration data from a limited number of sensors. *Mechanical Systems and Signal Processing*, 29:310–327, 2012.

[12] K. Maes, S. Gillijns, and G. Lombaert. A smoothing algorithm for joint input-state estimation in structural dynamics. *Mechanical Systems and Signal Processing*, 98:292–309, 2018.

[13] Kristof Maes, E Lourens, Katrien Van Nimmen, Edwin Reynders, Guido De Roeck, and Geert Lombaert. Design of sensor networks for instantaneous inversion of modally reduced order models in structural dynamics. *Mechanical Systems and Signal Processing*, 52:628–644, 2015.

[14] Saeed Eftekhar Azam, Eleni Chatzi, Costas Papadimitriou, and Andrew Smyth. Experimental validation of the Kalman-type filters for online and real-time state and input estimation. *Journal of Vibration and Control*, page 1077546315617672, 2015.

[15] K. Maes, K. Van Nimmen, E Lourens, A. Rezayat, P. Guillaume, G. De Roeck, and G. Lombaert. Verification of joint input-state estimation for force identification by means of in situ measurements on a footbridge. *Mechanical Systems and Signal Processing*, 75:245–260, 2016.

[16] Dionisio Bernal and Alessia Ussia. Sequential deconvolution input reconstruction. *Mechanical Systems and Signal Processing*, 50:41–55, 2015.

[17] Dionisio Bernal. Non-recursive sequential input deconvolution. *Mechanical Systems and Signal Processing*, 82:296–306, 2017.

[18] K. Maes, A.W. Smyth, G. De Roeck, and G. Lombaert. Joint input-state estimation in structural dynamics. *Mechanical Systems and Signal Processing*, 70:445–466, 2016.